Lithuanian Journal of Physics, Vol. **56**, No. 2, pp. 92–101 (2016)

INFLUENCE OF SURFACE PASSIVATION ON ELECTRIC PROPERTIES OF INDIVIDUAL GaAs NANOWIRES STUDIED BY CURRENT–VOLTAGE AFM MEASUREMENTS

P. Geydt [a], P.A. Alekseev [b], M.S. Dunaevskiy [b,c], T. Haggrén [d], J.-P. Kakko [d], E. Lähderanta [a], and H. Lipsanen [d]

[a] *School of Engineering Science, Lappeenranta University of Technology, P.O. Box 20, 53851 Lappeenranta, Finland*
[b] *Ioffe Physical Technical Institute, Politechnicheskaya 2, 194021 Saint Petersburg, Russia*
[c] *NRU ITMO, Kronverkskiy 49, 197101 Saint Petersburg, Russia*
[d] *Department of Micro- and Nanosciences, Micronova, Aalto University, P.O. Box 13500, FI-00076 Aalto, Finland*
E-mail: pavel.geydt@gmail.com

Received 8 January 2016; revised 8 March 2016; accepted 21 June 2016

Current–voltage (I–V) characteristics of vertical p-GaAs nanowires (NWs) covered by different surface passivation materials were experimentally measured by conductive atomic force microscopy (C-AFM). The obtained *I–V* curves for individual NWs with a diameter of 100 nm covered with AlGaAs, GaN, GaP or InP shell layers were compared to analyse the influence of surface passivation on the density of surface states and choose the most beneficial passivating material for technological applications. We have found the absence of a Schottky barrier between the golden catalytic cap on the top of a NW and the nanowire situated below and covered with an ultrathin GaP passivating layer. It was suggested that passivating material can arrange the heterostructure configuration with the GaAs NW near the Au cap. The latter mechanism was proposed to explain a strong energy barrier found in nanowires covered with InP passivation. AlGaAs passivation affected the forward threshold voltage of nanowires for NWs, which was measured simultaneously with the resistivity of each individual vertical structure from an array by means of AFM in the regime of measuring the I–V curves and onefold calculations. We made an attempt to develop the methodology of measurement and characterization of electric properties of passivated NWs.

Keywords: nanowires, passivation, GaAs, AFM, current–voltage characteristics

PACs: 73.43.Fj, 81.05.Ea, 81.07.Gf

1. Introduction

Group III–V semiconductor nanowires (NWs) have been extensively investigated during the last two decades due to their prospective application in multiple emerging NW-based devices [1]. Particularly, GaAs NWs are one of the most studied representatives of that class, since they are considered to be promising building blocks for next generation light emitting diodes [2], transistors [3], photodetectors [4] and photovoltaic cells [1, 5].

Nanowires are quasi one-dimensional structures. Their surface-to-volume ratios are considerably high, while the surface–diameter ratio is also high, which leads to an increase of the influence of surface effects on the NW's electronic properties. The high density of surface states, where electrons and holes can recombine (in GaAs NWs) [6], leads to the near surface depletion and significant decrease in an electrical current through NW, due to immobilization of holes on the surface for p-type GaAs. Moreover, charges can become trapped on surface states, causing local shifts in the electric potential. Surface passivation is used to eliminate these effects. Surface passivation consists of reducing the density of surface states and forming of a protective shell around the NW. Such passivation is necessary for GaAs NWs with diameters less than 150 nm [1], because it reduces the surface recombination rate and can increase the thickness of an undepleted area in the NW.

A limited number of parameters can be accessed to adjust the charge carriers' transport properties in NWs, e. g. effective diameter, height, surrounding media, size of the metal cap and passivation of the surface [7, 8]. More specifically, diameter/height and diameter/spacing correlations were postulated

theoretically by Hu [9] and Kupec [10], while optically transparent SiO_2 (usually surrounding the NW array in solar cells) can itself act as a passivating agent for surface states [11]. Furthermore, it is necessary to take into account the doping level and the interface between the bulk semiconductor material of a NW and the metal cap on its top. The latter exists due to a standard growth technique, since vertical NWs are usually fabricated by growing under the melted Au or Ga droplets. Unfortunately, such metal–semiconductor interface causes the Schottky junction and corresponding energy barrier [12–14].

As recently found by Wilks' group [15], the mechanisms of conductive performance for ZnO NWs can be shifted from diode-like to ohmic-like by size of an Au cap on the top of the NW, or more correctly by the relation of diameters of a metal cap and a NW. Interestingly, in their essential work a multi-probe contact device was utilized, although the results apply to the case of heavily doped NWs with a carrier concentration of approximately 10^{18} cm^{-3}.

Since passivation is necessary for GaAs due to a significantly high density of the surface states, a few articles recently reported studies of specific types of passivation layers for GaAs NWs. Surface passivation shells were found to exhibit a dissimilar stability and impact in conductive properties for AlGaAs [8, 16–19], AlInP [20, 21], InP [22], GaP [11, 22, 23], GaAsP [24] nitride chemical solution [25] and sulfur chemical solution [25–277] passivations. However, no effort to summarize these data has been made, and the majority of these works have utilized only non-contact techniques or procedures, where the signal was spatially averaged for the whole array of NWs.

Additionally, a few reports [22, 25] have already postulated that even an ultrathin layer of passivating material (<1 nm) can significantly increase the mobility of charge carriers and decrease the scattering of charge carriers on surface states. Therefore, the aim of our study was to compare different types of surface passivations on GaAs NWs and to establish the abilities of modern scanning probe methods to solve this task on individual vertical structures.

2. Samples and experimental methods

Fabrication of crystalline doped semiconductor nanowires was done by the vapour–liquid–solid (VLS) method. The doping level of the utilized zinc-doped GaAs substrate was ~1.4×10^{19} cm^{-3}, so its resistance was specially arranged to be ~7 Ω, i. e. few orders of magnitude higher than the conductivity expected for NWs. Thus, resistivity of such p^+-GaAs substrates is considered negligible and not affecting the measured *I–V* curves of NWs.

2.1. Fabrication of passivated p-doped GaAs NWs on p^+-GaAs substrates

The GaAs substrates were first cleaned using acetone, isopropanol and deionized water. The cleaned substrates were treated with poly-L-lysine, followed by ~100 nm Au nanoparticle deposition from a colloidal solution. Next, the substrates were placed in a metalorganic vapour phase epitaxy (MOVPE) reactor. Prior to nanowire growth, the samples were heated to 650 °C under H_2 flow for 10 minutes to desorb surface oxides. The temperature was then lowered to 450 °C for nanowire growth, which was performed by simultaneously opening trimethylgallium (TMGa) (6.1 μmol/s) and tertiarybutylarsine (TBAs) (114 μmol/s) flows. For passivation, ultrathin InP or GaP capping layers were grown in the same run using trimethylindium (TMIn) tertiarybutylphosphine (TBP) [22]. Alternatively, AlGaAs shells were grown at 650 °C by introducing TMGa, TBAs and trimethylaluminum (TMAl) flows of 9.2, 148 and 7.2 μmol/s, respectively. The AlGaAs shell growth times were 2, 5 and 20 s. The nanowires were additionally p-type doped with diethylzinc (DEZn), with flows of 0.1 μmol/s for all samples besides the sample with the AlGaAs shell grown during 20 s, for which the DEZn flow was 0.05 μmol/s during the NW growth.

Switching of the Ga and As sources in the preset protocol initiated the deposition of crystallites from the three-phase boundary (TPB) at the interface between a liquid Au droplet and a solid GaAs substrate [28]. Growth of the NWs in the (111B) crystal plane was continued until NWs have reached ~1 um in height (above the substrate, not considering the height of the Au cap). Deposition of the vapours on sidewall surfaces by the vapour–solid mechanism was not considered, though it usually leads to an increase of the diameter of the NW resulting in a slightly conical shape of NWs, i. e. wider at the bottom. GaAs NWs were further considered cylindrical with a GaAs core diameter of 100 nm. The thickness of shell passivation layers were considered equal for all NWs in each array and along the length of the vertical structures. The summarized data for the prepared samples is given in Table 1.

As mentioned above, the doping level of the NWs was controlled by additional DEZn flow and by adjusting the II/III ratio of Zn/Ga sources. For samples 1–6 (focused on comparison of passivation agents) the flow was 1 SCCM (standard cubic centimeters per minute) in order to reach ~10^{18}–10^{19} cm^{-3} [29].

It should be noted that sample 7 has been doped to an approximately twice lower level of ~0.5·(10^{18}–10^{19}) during the 0.5 SCCM flow, with the motivation to compare the *I*–*V* characteristics for GaAs NWs having different levels of doping. Heights and diameters of the fabricated p-GaAs NWs and their Au caps were controlled by a scanning electron microscope (SEM) after the growth. Further, all specified heights, diameters and doping levels were verified by AFM methods.

Table 1. Summarized parameters of seven studied samples of passivated p-GaAs NWs.

Sample	Passivation material	Thickness of the shell passivation layer	Doping level, cm^{-3}	Height of the NW, μm
1	(unpassivated)	–	10^{19}	1
2	GaP	~One monolayer	10^{19}	1
3	InP	Few monolayers	10^{19}	1
4	GaN	One monolayer	10^{19}	~0.4
5	AlGaAs	10 nm	10^{19}	1
6	AlGaAs	30 nm	10^{19}	1
7	AlGaAs	~300 nm	0.5·(10^{19})	1

Reference sample 1 was not passivated, while the passivating layers of samples 2, 3, 5, 6, 7 were grown in a MOVPE chamber by the vapour–solid mechanism. GaP and InP passivation layers were grown with thicknesses even less than 1 nm. Passivation with AlGaAs has been performed during different duration of precursor's flow, which led to the 10, 30 and ~300 nm thickness of the passivation layer, respectively (Fig. 1). The nitride passivation was done with liquid phase deposition by exposure of the array to a concentrated hydrazine solution during 5 minutes. Then, the stabilized GaN-coated sample was rinsed in double-distilled water and dried in air. The expected thickness of passivation is one monolayer of the GaN compound covering the NW [25]. Unfortunately, such treatment of the array by the liquid solution resulted in the observation that NWs became broken and the persistent height of the structures was ~400 nm. It can be expected due to the fact that a substrate with an array of NWs usually indicates low wettability by hydrophilic agents like hydrazine. This caused considerably high forces acting upon slim NWs in the array due to the weight of liquid hydrazine droplets. As a result, heights of the NWs were equal and Au caps were lost, so *I*–*V* curves were further measured via the connection between a metallized AFM probe and a semiconductor remainder of p-GaAs NW.

The SEM images and 3D-AFM images in Fig. 1(a–c, e) are displayed with a tilt angle of 30 degrees, in order to demonstrate the informativeness of these two microscopic methods. A pyramidal shape of the NWs, as seen on the AFM images, is explained by

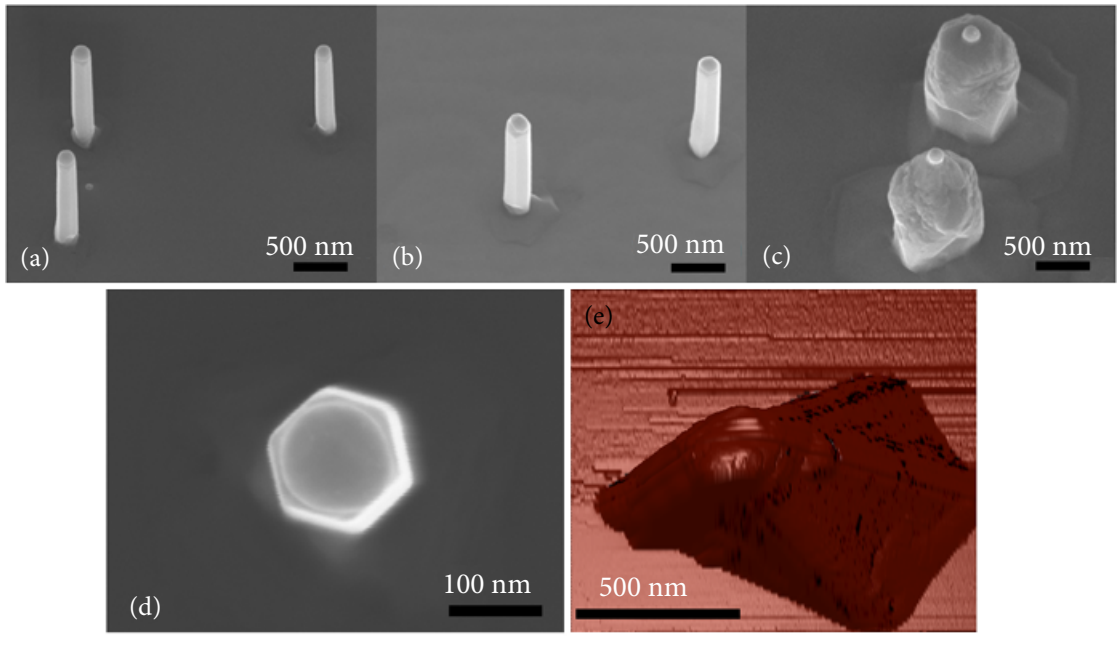

Fig. 1. SEM images of p-GaAs NWs covered with shell layers of AlGaAs passivations: (a) 10 nm, (b) 30 nm and (c) 300 nm. (d) SEM image of a cross-sectional profile of sample 5, top view. (e) The overlay of a conductivity map on 3D topography of sample 5 taken by AFM (coloured online).

the convolution of shapes of a slim vertical NW and a pyramidal shape of the tip of the AFM probe [16]. The diameter of the Au cap in Fig. 1(d) is 118 nm, while the distance between two parallel sides of the hexagon is 146 nm. This is caused partially by a small variability in the size of caps and by the shape of the NW resembling a hexagonal frustrum.

2.2. Methodology of the experiment

It is possible to notice that the map of conductivity indicates only few places where the PeakForce TUNA module of Multimode 8 AFM (*Bruker*) has recorded the conductive zones. This effect is in accordance with the properties of an AFM probe, considering the geometry of a certain AFM probe mounted on a flexible cantilever and the difference in conductivity for facets of the pyramid of the AFM probe. Thus, only one facet of the conductive probe's tip should be used for investigation of *I*–*V* curves for the whole set of studied samples.

In the C-AFM experiment, tracking of the topography and "mapping" of the electrically conductive zones were conducted simultaneously. This resulted in obtaining of the accurate coordinates of all NWs, positioning of their Au caps and locations of the zones with the highest currents, which were recorded on the right from the Au caps. Afterwards, measurements of the DC in *I*–*V* characteristics were done in the spots with the highest peak current (visible as black spots in Fig. 1(e)), instead of the Au cap coordinates. This implies that the most stable contact between the probe of an AFM device and the Au cap of a NW can be acquired in a particular contact geometry. Moreover, it is needed to consider the following: (1) partial wearing of the conductive Pt/Ir coating from the sectors of the AFM probe's tip, which arises due to delayed triggering of an AFM piezo scanner feedback loop (causing momentarily excessive forces of interaction between a probe and a NW); and (2) probability of uneven thickness of conductive coating, which leads to current flowing via a less resistive part of the probe (where conductive coating is thicker) instead of the AFM probe tip's apex.

Details of the contact between the probe and the sample are schematically presented in Fig. 2(a), where the three following angles can be seen: (1) an incline angle of the cantilever in the microscope probe holder (12°); (2) an additional angle of bending of the cantilever due to its flexibility (1°); and (3) an angle of pyramid's edge for PFTuna (*Bruker*) probes (15°). Considering vertically standing structures (90°), the NWs experienced the strongest stable mechanical interaction only with two facets of the pyramid of the AFM probe with the shallowest slope. Moreover, considering the inequality of thickness and the sturdiness of the conductive Pt/Ir coating, only one of these facets is preferable. As a result, it is necessary to find and choose this facet experimentally for each unique AFM probe, despite the expectations that probes are manufactured in compliance with the same industrial standards. For our investigation, it was possible to reveal that the upper-right quadrant of the pyramid indicated the highest local currents. Thus, the corresponding facet of the AFM probe was conceived as the most conductive and it has been further utilized to measure the *I*–*V* curves. It must be clarified that *I*–*V* measurements were done not via an AFM probe tip's apex,

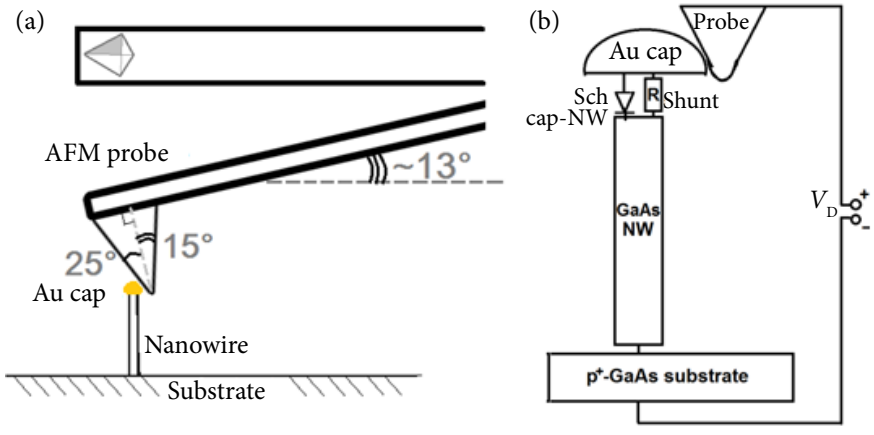

Fig. 2. (a) Experimental scheme indicating the geometry of the contact between an AFM pyramidal tip and a vertical NW, where the most conductive facet is shaded. (b) Equivalent electric circuit for the measured system. Resistances of the substrate, Au cap, probe and probe-cap area are considered negligible, while the resistance of the shunt is considerably high.

because the contact resistance would be drastically enlarged for a thin conductive coating of the apex and a small surface area of the contact between the AFM probe and the NW cap. With this in mind, it becomes clear that despite the observance of the conductive regions at distances of tens of nanometres from the Au caps (see the upper-right side of the pyramid in Fig. 1(e) and the sketch in Fig. 2(a)), the *I*–*V* measurements of p-GaAs NWs have been carried out solely via their Au caps. Consequently, the contact between the metallized AFM probe and the Au cap was ohmic (see an equivalent circuit in Fig. 2(b)).

These issues were taken into account during the measurements of *I*–*V* curves, with regard to AFM controller's accuracy of measuring the electrical currents. The PeakForce TUNA feedback module allows measuring the currents up to 500 nA with a precision step as low as 375 fA and an accuracy of <100 fA, which is suitable for the measurements of conductivity even for NWs with a significantly lower doping level (~10^{15} cm^{-3}) than for our materials. The module is capable to induce the electric potential in the range between –10 and 10 V with the principal accuracy step of ~0.31 mV.

3. Results

Passivation can be considered stable, because all NWs were kept in standard room conditions during 3 months before C-AFM measurements and were still highly conductive. We present the obtained data on *I*–*V* curves with a precision of 37.5 pA and 11.7 mV. Different regions of Schottky diode characteristics for the series of seven samples were observed. In order to compare these *I*–*V* curves, we collected data for each type of passivation on a repeatable basis for 3–7 separate NWs from different locations on each sample. The measured NWs had distinctions due to a small variation of diameters in the fabricated NWs, that affected the nominal diameter of the conductive channel, i. e. the effective diameter. *I*–*V* curves for NWs with different types of passivation are presented in Figs. 3 and 4 without filtering of the obtained signals.

Let us analyze them on the basis of the model given by Ellis in [30] and an equivalent electrical circuit from Fig. 2(b). The diode law describing the conductive performance of a Schottky diode is an exponential relation between the current through the diode *I* and the bias voltage *V*:

$$I = I_0 \cdot (e^{eV/kT} - 1), \quad (1)$$

where I_0 is the reverse-bias leakage current, the elementary charge $e = 1.6 \cdot 10^{-19}$ C, $k = 1.23 \cdot 10^{-23}$ J/K and *T* is the absolute temperature.

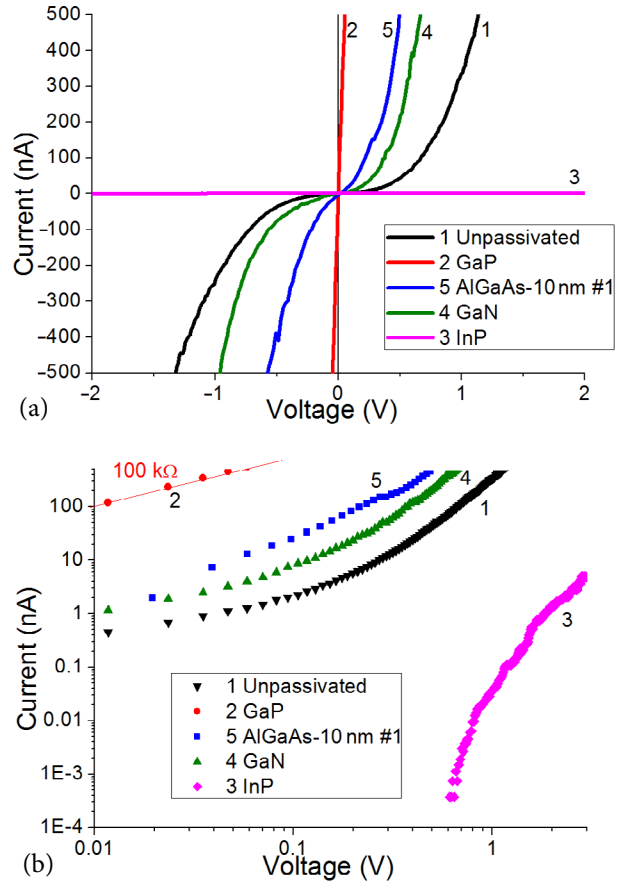

Fig. 3. Comparison of *I*–*V* curves for p-GaAs NWs covered by four studied types of surface passivation. *I*–*V* curves (coloured online) are given in (a) linear and (b) double logarithmic scales for the region of forward bias. Sample numbers indicated near the curves are referred to the samples in + 1.

Therefore, it seems beneficial to represent data complementarily in logarithmic scales, revealing the value of characteristic threshold voltage, as it is approximately the voltage of the intersection of *I*–*V* curves with an *x* axis for samples 6 and 7 in our series. Additionally, it demonstrates the shunting mechanism of nanowires with parallel series of a diode and a resistor [30, 31], where shunting diode's threshold voltage is high, while its corresponding parallel resistance is small. Such leakage should lead to a slowly increasing Log(*I*) up to a specific voltage region, where the main diode becomes opened causing a linear Log(*I*) segment, and a further part of the curve demonstrates the bending of the curve into the linear resistance region. The incline of the latter almost linear region can be recalculated into the resistivity of the nanowire at the highest Log(*I*) values in Fig. 4(b) [30].

When the Schottky diode is in the forward mode, the NW does not conduct current until the forward voltage exceeds a certain value, i. e. the forward

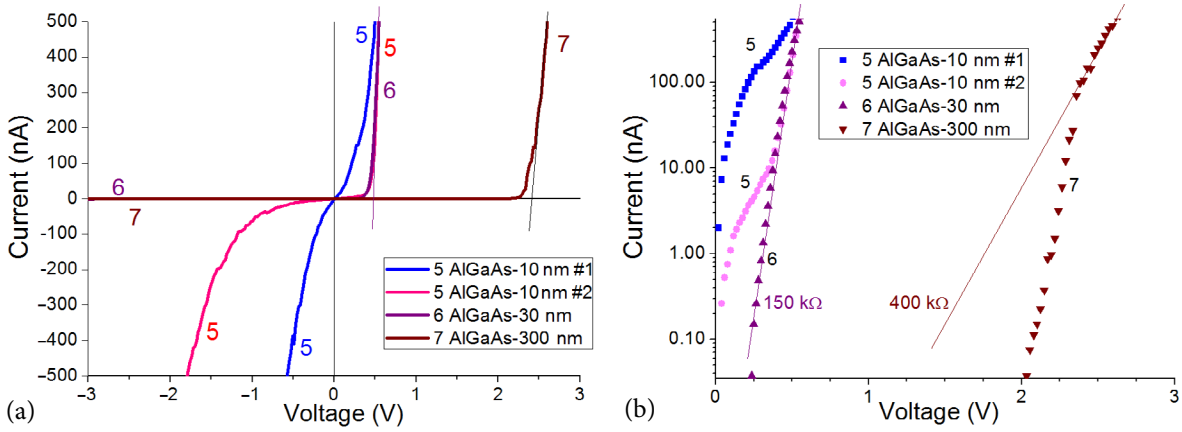

Fig. 4. Comparison of p-GaAs NWs covered with AlGaAs shell layers for samples 5–7 (coloured online). Electrical characteristics are given in (a) linear and (b) semi logarithmic scales for the quadrant with forward bias. Two separate NWs are represented for sample 5.

threshold voltage V_T. All the current visible for the NW in the region of small potential difference is the leakage current, which is due to the parasitic shunt connection between the Au cap and GaAs material. It can reach hundreds of nanoamperes already at 0.5 V as it was visible for sample 5, even though resistivity of this shunt element is considerably high (usually $\gg$1 MΩ).

Reference sample 1 represents the NW with a noticeable transition from the shunted region to the diode. NWs with nitride passivation have shown an increase in the measured current compared to that of the unpassivated sample. However, the shown *I*–*V* curves for sample 4 are representative of a 0.4 μm high remainder of the NW without an Au cap. Consequently, a visible Schottky barrier has been caused by the metal–semiconductor interface between the conductive coating of the AFM and the upper part of the passivated p-GaAs NW. It is also probable that a negligible tunnelling barrier persists on the *I*–*V* curves, although the thickness of the GaN layer responsible for it was approximately one monolayer [25]. A nitride cover layer of passivation cannot grow thicker than one monolayer due to the significant lattice mismatch between zinc-blende GaAs and wurtzite GaN. Despite the mentioned changes in NW parameters, the decrease of NW's height should result only in a change of incline of the *I*–*V* curves, but not its shape. This consideration leads to the conclusion that nitride passivation has moderate performance, while its high efficiency is supported by the previous results [25].

GaP-passivation on the surface of GaAs NWs caused the complete absence of a Schottky barrier, so the *I*–*V* curves appeared to have an almost linear shape for sample 2. This demonstrates the formation of the ohmic contact between the Au cap and p-GaAs NW. Consequently, the density of surface states became significantly decreased for the GaP-passivated sample. This record correlates with our previous results [11] and was reported by other authors [22, 23], where an increase of the measured electric current was established compared with that of the unpassivated sample. Resistivity of the NW can be calculated from the region of linear resistance, i. e. high potential in forward bias. For GaP-passivated p-GaAs NWs in our study, R_{NW} was ~10^5 Ω. This value is comparable to the theoretical expectation for resistivity $R \sim 2 \cdot 10^5$ Ω of a GaAs NW at 300 K evaluated from the following formula:

$$R = L/(e \cdot N_A \cdot \mu \cdot \pi r^2). \quad (2)$$

Here height $L = 1$ μm, elementary charge $e = 1.6 \cdot 10^{-19}$ C, doping level $N_A = 10^{19}$ cm^{-3}, mobility $\mu = 400$ cm^2/V·s and NW radius $r \sim 50$ nm.

InP-passivated sample 3 demonstrated a surprisingly low electric current on the *I*–*V* curves. Direct current was measured to be approximately 3 nA under the 7 V external bias of both polarities, which is much less than that for the unpassivated sample 1. According to these results, a very strong energy barrier was observed for InP passivated p-GaAs NWs. It would seem that InP increase the amount of surface states so that a passivating layer has a drastically adverse effect. However, photoluminescence spectroscopy has shown opposite results for similar samples [22]. An assumption that the connection between the AFM probe and the Au caps was not properly established exactly on InP-passivated NWs has been rejected after observation of the same effect on multiple separate NWs on sample 3 by few fresh AFM probes, which were further used to study other types of passivation layers by the same protocol, i. e. taking into account

equal force, scanning probe's velocity, voltage range etc. These findings require a detailed investigation and modelling.

A highly interesting result has been obtained for p-GaAs NWs with AlGaAs passivation, i. e. a noticeable increase in the current compared with unpassivated NWs. It was found that shunt resistance can vary among the NWs in one array (see two data curves for sample 5 in Fig. 4). This effect can similarly be attributed to the difference in the diameters of Au caps. It is also possible to explain the difference in the measured characteristics after considering the local changes in the thickness of the passivating layer (see Fig. 1(d)). This could lead to fluctuation in surface potentials and affect the height of a Schottky barrier and the effective diameter of a NW. By increasing the thickness of the AlGaAs core, local variations tend to align, so only the diode and internal forward resistance regions are seen for 30 nm. Further for a 300 nm thick NW, only the diode and the beginning of curvature for linear resistance are visible.

According to the incline of these segments of *I*–*V* curves, nanowires with higher doping have shown the resistance ~10^2 kΩ (samples 2, 5 or 6), compared to the resistance ~$4 \cdot 10^2$ kΩ measured for a low doped sample 7. To verify that the observed segments are corresponding to the mentioned regions of the Schottky diode curve, we can consider the doping levels of these NWs. After the calculations, it becomes clear that the experimentally evaluated resistance corresponds well with the values expected from Eq. (2), i. e. ~$2 \cdot 10^2$ kΩ (10^{19} cm^{-3}) and ~$4 \cdot 10^2$ kΩ ($0.5 \cdot 10^{19}$ cm^{-3}). Moreover, the difference in the resistance for samples 2, 5 or 6 and sample 7 is comparable with the difference of doping levels by the order of values. Furthermore, an increase in the thickness of the AlGaAs passivating layer shifted the characteristic forward the threshold voltage for NWs, which is seen from Fig. 4(a). The characteristic V_T is ~0.2 V for NW with a 30 nm thick passivating layer, while it increases up to ~2.4 V for the NW covered with a 300 nm ultra-thick AlGaAs shell.

4. Discussion

Comparison of the studied passivation types reveals that GaP surface passivation is the most effective to eliminate the Schottky barrier input in GaAs NWs. We have observed that no barriers exist in the *I*–*V* curves on nanowires covered already by an ultrathin GaP layer. It can be suggested that GaP passivated NWs have a shunt, although it is not correct. Indeed, previously we have studied the properties of NWs with a similar geometry, passivating layer and doping level, but with n-type doping on p^+-GaAs, i. e. pn-junction, combined with a Schottky barrier [11]. In the case of shunting, it would represent an ohmic-like curve or a Schottky-like curve, while linear resistance should remain similar. We have not observed any shunted NWs for that series, because all of the NWs represented the characteristic pn-junction shape of the *I*–*V* curves. Since these two discussed systems are similar, we conclude that the series of GaP-passivated NWs studied in a recent paper did not have shunts. Similar results for high performance of GaP-passivated GaAs NWs are reinforced by results from other methods [22, 23], including comprehensive theoretical interpretation [6]. A reduced Fermi-level pinning was previously suggested as a possible explanation for lowering of Schottky barriers at metal-catalyst/NW interfaces. Authors explained the barrier lowering by a reduced density of pinning states combined with a formation of an electric dipole layer [6]. Fortunately, here this effect has been recorded experimentally by the contact AFM technique, so that we could generalize the *I*–*V* curves to represent them in the log-scale and later qualitatively verify the resistivity of the p-GaAs NWs.

The difference in the adhesion of AlGaAs-passivation to a GaAs zinc-blende crystal might be considered and compared with other passivating materials. Taking into account the negligible lattice mismatch between GaAs and a thin layer of AlGaAs, it was possibly easier for AlGaAs passivation to cover the sidewalls. Referring to Fig. 1(d), such a hexagonal profile was observed only for 10 nm thick AlGaAs NWs by SEM, while other NWs in this study seemed considerably closer to a cone-shape rather than a shape resembling a hexagonal frustrum. Moreover, such resemblance in the properties of passivation and NW could result in acceleration of the VLS mechanism during the vapour source flow, so AlGaAs could partially crystallize between the Au cap and the GaAs NW, creating an additional tunnelling barrier.

It is possible to suggest that the assumption about the VLS mechanism is valid not only in the AlGaAs case but also for InP-passivation. In this architecture, the Schottky barrier can be shadowed by even stronger tunnelling barrier. However, the thickness of this possible layer was close to that of a monolayer. The heterojunction could result in decreasing of current, but this heterostructure should have a specific threshold voltage, while it was not observed in the voltage scan range from –7 to +7 V.

For GaN NWs, it is possible to quantify that the current increased ~6 times, while the NW became 2.5 times shorter. A thin layer of GaN on the top of the NW between the AFM probe and GaAs NW

could result in a negligible tunnel barrier, which can hardly be visualized by our technique.

Summarizing these ideas about passivation, it appears that different types of surface passivation can be used to change the properties of the desired NW. Decrease of the Schottky barrier between the Au cap and the semiconductor nanowire can be observed and evaluated by intersection of the logarithm of DC with the axis of applied potential bias. Simultaneously, the incline of the logarithmic curve at the region of serial resistance, which emerges after the linear diode region, is responsible for the resistivity of the nanowire. All these valuable data can be acquired with a proper operational protocol in room conditions with a single device, *viz.* a scanning probe station equipped with the facility to measure the direct electric current.

It should be noted here that photoluminescence (PL) studies made earlier on similar InP-doped materials did not reveal undesirable effects of InP passivation on the GaAs NWs [22]. Thus, it seems interesting to highlight the advantage of the scanning probe method, due to its ability to verify the conductive properties and the existence of the Schottky junction in the nanowire by a clear repeatable and gentle physical contact. AFM can be used to qualify multiple individual structures during only a few-minute study [32]. The C-AFM PFTuna module can be successfully used for the measurements of significantly low currents as in our work.

Furthermore, we consider the essential benefit of such AFM technique due to the concept that this method can be developed to carry out the studies of desired nanowires in the programmed automated basis already in the nearest perspective [33]. Several works [15, 34, 35] appeared concerning (a) visualization of a scanning probe during conductive measurements, (b) *in situ* adjustments or the so-called image pattern recognition techniques, and (c) multiple probe operation by a scanning probe station. They can be further combined into a fast comprehensive tool to study separate nanowires by precise contact measurements on AFM.

Summarizing these reports about the method, further advances in AFM techniques are possible. Establishing of comprehensive parameters of the contact between an AFM probe and a vertical NW is still necessary. Specific features of *I–V* curves related to a single individual NW can help one to confine the fabrication procedures and technological quality of semiconductor nanowires for novel solar cells, diodes and photodetectors, among other applications, on a developed and fast basis. We have proven the possibility of carrying such research on fragile vertical NWs by means of a standard device in room conditions.

5. Conclusions

In conclusion, adjustments of the electric parameters of nanowire-based devices become possible by implementation of a particular passivation layer on their surface and a proper level of doping. GaP has been found to be the most effective passivating agent for GaAs nanowires. While doping itself increases the amount of charge carriers and decreases the resistivity of the structure, passivation can be used to eliminate the Schottky barrier and therefore to increase the conductivity at the region near the zero external bias. Both these factors enhance the current through the nanowire, which can be observed by conductive AFM on individual nanostructures. The region of shunting resistance and internal forward resistance of the nanowires can be distinguished with the corresponding forward threshold voltages. Such developed procedure is proposed to be utilized at the design control stage to enhance the properties of recently emerging nanodevices.

Acknowledgements

We would like to thank Prof. V.L. Berkovits for arranging the nitride passivation. The reported study was funded by RFBR according to the Research Project 16-32-60147 mol_a_dk.

References

[1] R.R. LaPierre, A.C.E. Chia, S.J. Gibson, C.M. Haapamaki, J. Boulanger, R. Yee, P. Kuyanov, J. Zhang, N. Tajik, N. Jewell, and K.M.A. Rahman, III–V nanowire photovoltaics: Review of design for high efficiency, Phys. Status Solidi RRL **7**, 815–830 (2013), http://dx.doi.org/10.1002/pssr.201307109

[2] V.G. Dubrovskii, G.E. Cirlin, and V.M. Ustinov, Semiconductor nanowhiskers: Synthesis, properties, and applications, Semiconductors **49**, 1539–1584 (2009), http://dx.doi.org/10.1134/S106378260912001X

[3] X. Miao, K. Chabak, C. Zhang, P.K. Mohseni, D. Walker Jr., and X. Li, High-speed planar GaAs nanowire arrays with $f_{max} > 75$ GHz by wafer-scale bottom-up growth, Nano Lett. **15**, 2780–2786 (2015), http://dx.doi.org/10.1021/nl503596j

[4] X. Dai, S. Zhang, Z. Wang, G. Adamo, H. Liu, Y. Huang, C. Couteau, and C. Soci, GaAs/AlGaAs nanowire photodetector, Nano Lett. **14**, 2688–2693 (2014), http://dx.doi.org/10.1021/nl5006004

[5] J.V. Holm, H.I. Jørgensen, P. Krogstrup, J. Nygård, H. Liu, and M. Aagesen, Surface-passivated GaAsP single-nanowire solar cells exceeding 10% efficiency grown on silicon, Nat. Comm. **4**, 1498 (2013), http://dx.doi.org/10.1038/ncomms2510

[6] D.B. Suyatin, V. Jain, V.A. Nebol'sin, J. Trägårdh, M.E. Messing, J.B. Wagner, O. Persson, R. Timm, A. Mikkelsen, I. Maximov, L. Samuelson, and H. Pettersson, Strong Schottky barrier reduction at Au-catalyst/GaAs-nanowire interfaces by electric dipole formation and Fermi-level unpinning, Nat. Comm. **5**, 3221 (2014), http://dx.doi.org/10.1038/ncomms4221

[7] T. Hanrath and B.A. Korgel, Chemical surface passivation of Ge nanowires, J. Am. Chem. Soc. **126**, 15466–15472 (2004), http://dx.doi.org/10.1021/ja0465808

[8] J.L. Boland, S. Conesa-Boj, P. Parkinson, G. Tütüncüoglu, F. Matteini, D. Rüffer, A. Casadei, F. Amaduzzi, F. Jabeen, C.L. Davies, H.J. Joyce, L.M. Herz, A.F. i Morral, and M.B. Johnston, Modulation doping of GaAs/AlGaAs core–shell nanowires with effective defect passivation and high electron mobility, Nano Lett. **15**, 1336–1342 (2015), http://dx.doi.org/10.1021/nl504566t

[9] L. Hu and G. Chen, Analysis of optical absorption in silicon nanowire arrays for photovoltaic applications, Nano Lett. **7**, 3249–3252 (2007), http://dx.doi.org/10.1021/nl071018b

[10] J. Kupec, R.L. Stoop, and B. Witzigmann, Light absorption and emission in nanowire array solar cells, Opt. Express **18**, 27589–27605 (2010), http://dx.doi.org/10.1364/OE.18.027589

[11] P. Geydt, P.A. Alekseev, M.S. Dunaevskiy, T. Haggrén, J.-P. Kakko, E. Lähderanta, and H. Lipsanen, Observation of linear *I*–*V* curves on vertical GaAs nanowires with atomic force microscope, J. Phys. Conf. Ser. **661**, 012031 (2015), http://dx.doi.org/10.1088/1742-6596/661/1/012031

[12] E. Koren, N. Berkovitch, O. Azriel, A. Boag, Y. Rosenwaks, E.R. Hemesath, and L.J. Lauhon, Direct measurement of nanowire Schottky junction depletion region, Appl. Phys. Lett. **99**, 223511 (2011), http://dx.doi.org/10.1063/1.3665182

[13] C.-H. Hsu, Q. Wang, X. Tao, and Y. Gu, Electrostatics and electrical transport in semiconductor nanowire Schottky diodes, Appl. Phys. Lett. **101**, 183103 (2012), http://dx.doi.org/10.1063/1.4765653

[14] Y. Jiao, A. Hellman, Yu. Fang, S. Gao, and M. Käll, Schottky barrier formation and bending revealed by first-principles calculations, Sci. Rep. **5**, 11374 (2015), http://dx.doi.org/10.1038/srep11374

[15] A.M. Lord, Th.G. Maffeis, O. Kryvchenkova, R.J. Cobley, K. Kalna, D.M. Kepaptsoglou, Q.M. Ramasse, A.S. Walton, M.B. Ward, J. Köble, and S.P. Wilks, Controlling the electrical transport properties of nanocontacts to nanowires, Nano Lett. **15**, 4248–4254 (2015), http://dx.doi.org/10.1021/nl503743t

[16] P.A. Dementyev, M.S. Dunaevskii, Yu.B. Samsonenko, G.E. Cirlin, and A.N. Titkov, Current–voltage characteristics of silicon-doped GaAs nanowhiskers with a protecting AlGaAs coating overgrown with an undoped GaAs layer, Semiconductors **44**, 610–615 (2010), http://dx.doi.org/10.1134/S1063782610050118

[17] C.-C. Chang, C.-Y. Chi, M. Yao, N. Huang, C.-C. Chen, J. Theiss, A.W. Bushmaker, S. LaLumondiere, T.-W. Yeh, M.L. Povinelli, C. Zhou, P.D. Dapkus, and S.B. Cronin, Electrical and optical characterization of surface passivation in GaAs nanowires, Nano Lett. **12**, 4484–4489 (2012), http://dx.doi.org/10.1021/nl301391h

[18] O. Demichel, M. Heiss, J. Bleuse, H. Mariette, and A. Fontcuberta i Morral, Impact of surfaces on the optical properties of GaAs nanowires, Appl. Phys. Lett. **97**, 201907 (2010), http://dx.doi.org/10.1063/1.3519980

[19] L.V. Titova, T.B. Hoang, H.E. Jackson, L.M. Smith, J.M. Yarrison-Rice, H.J. Joyce, H.H. Tan, and C. Jagadish, Temperature dependence of photoluminescence from single core-shell GaAs–AlGaAs nanowires, Appl. Phys. Lett. **89**, 173126 (2006), http://dx.doi.org/10.1063/1.2364885

[20] A.C. Chia, M. Tirado, Y. Li, S. Zhao, S. Mi, D. Comedi, and R.R. LaPierre, Electrical transport and optical model of GaAs-AlInP core-shell nanowires, J. Appl. Phys. **111**, 094319 (2012), http://dx.doi.org/10.1063/1.4716011

[21] A.C. Chia, M. Tirado, F. Thouin, R. Leonelli, D. Comedi, and R.R. LaPierre, Surface depletion and electrical transport model of AlInP-passivated GaAs nanowires, Semicond. Sci. Technol. **28**, 105026 (2013), http://dx.doi.org/10.1088/0268-1242/28/10/105026

[22] T. Haggren, H. Jiang, J.-P. Kakko, T. Huhtio, V. Dhaka, E. Kauppinen, and H. Lipsanen, Strong surface passivation of GaAs nanowires with ultrathin InP and GaP capping layers, Appl. Phys. Lett. **105**, 033114 (2014), http://dx.doi.org/10.1063/1.4891535

[23] A. Darbandi, O. Salehzadeh, P. Kuyanov, R.R. LaPierre, and S.P. Watkins, Surface passivation of tellurium-doped GaAs nanowires by GaP: Effect on electrical conduction, J. Appl. Phys. **115**, 234305 (2014), http://dx.doi.org/10.1063/1.4883960

[24] A. Lin, J.N. Shapiro, P.N. Senanayake, A.C. Scofield, P.-S. Wong, B. Liang, and D.L. Huffaker, Extracting transport parameters in GaAs nanopillars grown by selective-area epitaxy, Nanotechnol. **23**, 105701 (2012), http://dx.doi.org/10.1088/0957-4484/23/10/105701

[25] P.A. Alekseev, M.S. Dunaevskiy, V.P. Ulin, T.V. Lvova, D.O. Filatov, A.V. Nezhdanov, A.I. Mashin, and V.L. Berkovits, Nitride surface passivation of GaAs nanowires: impact on surface state density, Nano Lett. **15**, 63–68 (2015), http://dx.doi.org/10.1021/nl502909k

[26] N. Tajik, Z. Peng, P. Kuyanov, and R.R. LaPierre, Sulfur passivation and contact methods for GaAs nanowire solar cells, Nanotechnol. **22**,

225402 (2011), http://dx.doi.org/10.1088/0957-4484/22/22/225402

[27] N. Tajik, A.C.E. Chia, and R.R. LaPierre, Improved conductivity and long-term stability of sulfur-passivated n-GaAs nanowires, Appl. Phys. Lett. **100**, 203122 (2012), http://dx.doi.org/10.1063/1.4719675

[28] L. Chen, W. Lu, and C.M. Lieber, in: *Semiconductor Nanowires: From Next-Generation Electronics to Sustainable Energy*, eds. W. Lu and J. Xiang (Royal Society of Chemistry, United Kingdom, 2014) pp. 1–53, http://dx.doi.org/10.1039/9781782625209-00001

[29] Ch. Gutsche, I. Regolin, K. Blekker, A. Lysov, W. Prost, and F.J. Tegude, Controllable *p*-type doping of GaAs nanowires during vapor–liquid–solid growth, J. Appl. Phys. **105**, 024305 (2009), http://dx.doi.org/10.1063/1.3065536

[30] J.A. Ellis and P.A. Barnes, Current–voltage characteristics of a GaAs Schottky diode accounting for leakage paths, Appl. Phys. Lett. **76**, 124–125 (2000), http://dx.doi.org/10.1063/1.125677

[31] A. Fejfar, M. Hývl, M. Ledinský, A. Vetushka, J. Stuchlík, J. Kočka, S. Misra, B. O'Donnell, M. Foldyna, L. Yu, and P.R. Cabarrocas, Microscopic measurements of variations in local (photo)electronic properties in nanostructured solar cells, Sol. Energ. Mater. Sol. Cells **119**, 228–234 (2013), http://dx.doi.org/10.1016/j.solmat.2013.07.042

[32] A.X. Cartagena-Rivera, W.-H. Wang, R.L. Geahlen, and A. Raman, Fast, multi-frequency, and quantitative nanomechanical mapping of live cells using the atomic force microscope, Sci. Rep. **5**, 11692 (2015), http://dx.doi.org/10.1038/srep11692

[33] B. Torre, M. Bicego, M. Cristiani, V. Murino, A. Diaspro, and R. Cingolani, Combination of atomic force microscopy and principal component analysis as a general method for direct recognition of functional and structural domains in nanonocomposite materials, Microsc. Res. Tech. **73**, 973–981 (2010), http://dx.doi.org/10.1002/jemt.20837

[34] R. Timm, O. Persson, D.L.J. Engberg, A. Fian, J.L. Webb, J. Wallentin, A. Jönsson, M.T. Borgström, L. Samuelson, and A. Mikkelsen, Current–voltage characterization of individual as-grown nanowires using a scanning tunneling microscope, Nano Lett. **13**, 5182–5189 (2013), http://dx.doi.org/10.1021/nl402570u

[35] M. D'Acunto and O. Salvetti, Pattern recognition methods for thermal drift correction in Atomic Force Microscopy imaging, Pattern Recogn. Image Anal. **21**, 9–19 (2011), http://dx.doi.org/10.1134/S1054661811010056

PAVIRŠIAUS PASYVACIJOS ĮTAKOS PAVIENIŲ GaAs NANOVAMZDELIŲ ELEKTRINĖMS SAVYBĖMS TYRIMAS MATUOJANT SROVĖS PRIKLAUSOMYBĘ NUO ĮTAMPOS ATOMINĖS JĖGOS MIKROSKOPU

P. Geydt [a], P.A. Alekseev [b], M.S. Dunaevskiy [b,c], T. Haggrén [d], J.-P. Kakko [d], E. Lähderanta [a], H. Lipsanen [d]

[a] *Lapenrantos technologijos universitetas, Lapenranta, Suomija*

[b] *Jofės fizikos technikos institutas, Sankt Peterburgas, Rusija*

[c] *Valstybinis informacinių technologijų, mechanikos ir optikos universitetas, Sankt Peterburgas, Rusija*

[d] *Alto universitetas, Suomija*